Applied Catalysis B: Environmental 125 (2012) 324–330

Contents lists available at SciVerse ScienceDirect

Applied Catalysis B: Environmental

journal homepage: www.elsevier.com/locate/apcatb

Highly dispersed nickel loaded on mesoporous silica: One-spot synthesis strategy and high performance as catalysts for methane reforming with carbon dioxide

Zhicheng Liu[a,*], Jian Zhou[a,1], Kun Cao[b,1], Weimin Yang[a,b,**], Huanxin Gao[a], Yangdong Wang[a], Hexing Li[b]

[a] Shanghai Research Institute of Petrochemical Technology, SINOPEC Groups, 1658 Pudong Beilu, Shanghai 201208, PR China
[b] Life and Environment Science College, Shanghai Normal University, 100 Guilin Road, Shanghai 200234, PR China

ARTICLE INFO

Article history:
Received 23 February 2012
Received in revised form 5 June 2012
Accepted 8 June 2012
Available online 15 June 2012

Keywords:
Nickel
Mesoporous silica
Methane reforming with carbon dioxide
Catalysis

ABSTRACT

A kind of Ni containing mesoporous silica, Ni-KIT-6, was prepared by a one-spot co-assembly method, in which Ni species were highly dispersed into the pore walls during the self-assembly synthesis of the mesoporous silica. Compared with the catalyst prepared by conventional impregnation method, Ni-KIT-6 demonstrates extremely smaller Ni particles on the support and stronger interaction of Ni with silica matrix. As a result, it exhibits high catalytic activity and selectivity, and more importantly, good coke-resistant performance for the catalytic reaction of methane reforming with carbon dioxide.

1. Introduction

With the increase of global temperature, greenhouse effect has already attracted much attention in the last decade. How to deal with or utilize carbon dioxide and other greenhouse gases has become an important issue for both governments and scientists all over the world [1]. Catalytic reforming of methane with carbon dioxide, also known as dry reforming, is believed to be one of the feasible ways for simultaneous chemical transformation of two types of greenhouse gases, CO_2 and CH_4, to syngas, which can be used as feedstock for methanol production, Fischer–Tropsch synthesis or even Solid Oxide Fuel Cell (SOFC) [2], etc. However, CH_4–CO_2 reforming reaction is carried out at high temperature, and consequently suffers from coke formation on the catalysts, which poses a great challenge for its industrial application [3]. Therefore, the development of high performance catalysts is highly desired. Until now, lots of efforts focused on catalysts composed of noble metals or non-noble metals. Although noble metal catalysts have better anti-coke performance, group VIII metals, especially Ni-based catalysts are of more interests due to their much lower price than noble metal catalysts [3]. Unfortunately, they are more easily deactivated because of carbon deposition and active metal sintering. Recently, many improvements have been made to achieve higher catalytic activity and stability by controlling metal particle size to nanometer-scale and raising its dispersive distribution [4,5]. Moreover, metal particles should be loaded on supports with high surface areas, such as Al_2O_3 [5–7], ZrO_2 [8], MgO [9], ZrO_2–MgO [10], $Ce_{1-x}Gd_xO_2$ [2], SiO_2 [11] and mesoporous materials [12–16]. Particularly, mesoporous materials provide uniform channels to load active metal, and literaturely, mesoporous nanocrystalline zirconia supported nickel catalysts [12], Ni-supported MCM-41 catalysts [13], nickel-grafted MCM-41 [14], SBA-15 [14] and TUD-1 [15] mesoporous catalysts, and Ni-embedded mesoporous titania/silica [16] were subsequently reported. However, the performances of above-mentioned catalysts, especially the catalytic stabilities were still unsatisfied. One of the important reasons may be due to the relatively large nickel particle sizes (more than 10 nm in most reports), which are not small enough to achieve high anti-sinter and coke-resistance properties, as has ever been revealed by theoretical studies that if the Ni facets or step edges were small enough, nucleation of graphene could not proceed and graphite formation was further suppressed [17].

Herein, we prepared a kind of Ni-loaded catalyst (denoted as Ni-KIT-6) in which nano-sized Ni particles (less than 5 nm) were highly dispersed on pore walls of KIT-6, a kind of mesoporous silica with highly accessible and open pore networks. Ni-KIT-6 was

* Corresponding author. Fax: +86 21 68462283.
** Corresponding author at: Shanghai Research Institute of Petrochemical Technology, SINOPEC Groups, 1658 Pudong Beilu, Shanghai 201208, PR China. Fax: +86 21 68462283.
E-mail addresses: liuzc.sshy@sinopec.com (Z. Liu), yangwm.sshy@sinopec.com (W. Yang).
[1] These authors contributed equally to this work.

0926-3373/$ – see front matter © 2012 Elsevier B.V. All rights reserved.
http://dx.doi.org/10.1016/j.apcatb.2012.06.003

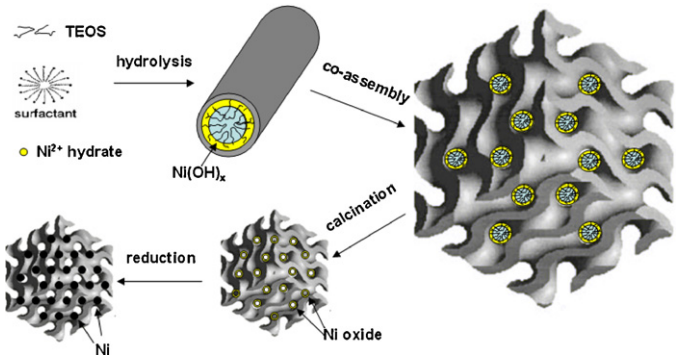

Fig. 1. A schematic diagram for the preparation of the Ni-KIT-6 catalyst.

synthesized by a one-spot co-assembly method, wherein Ni species were incorporated into the pore walls during the hydrothermal synthesis of mesoporous KIT-6 material. For better understanding of the synthesis procedure of Ni-KIT-6 catalysts, a schematic diagram was shown in Fig. 1. The synthesis process contains two key steps: co-assembly under the direction of surfactant, then calcination and reduction. Such novel catalyst exhibits high activity and prolonged lifetime in the dry reforming reaction compared with Ni supported KIT-6 sample (denoted as Ni/KIT-6), which was prepared by conventional incipient wetness impregnation method.

2. Experimental

2.1. Catalyst preparation

Ni-KIT-6 mesoporous materials were prepared by one-spot co-assembly method. The molar ratio of TEOS:P123:HCl:$Ni(NO_3)_2$:BuOH:H_2O was 1:0.017:1.83:(0.020–0.061):1.131:195. The mixture was stirred at 35 °C for 24 h, and then kept at 95 °C under static conditions for 48 h. The pH value of the solution was adjusted to 8–12 in advance. After that, solid products were collected by filtration, then dried overnight at 100 °C, and calcined in air at 550 °C for 6 h. The samples prepared were named as *x*Ni-KIT-6, where *x* is the mass content of nickel being 2.0%, 4.0% or 6.0%.

Ni/KIT-6 was prepared by conventional incipient wetness impregnation method as a reference. The preparation method was listed as follows: $Ni(NO_3)_2{\cdot}6H_2O$ was dissolved in deionized water, and then KIT-6 support was added into the solution. The mixture was stirred overnight at room temperature, then dried at 95 °C, and calcined in air at 550 °C for 6 h. We named the product as 6%Ni/KIT-6 in which the mass content of Ni was 6%.

2.2. Catalytic reaction

The catalytic properties of the catalysts for methane reforming with carbon dioxide were tested in a continuous-flow fixed-bed quartz reactor under atmospheric pressure. The internal diameter of the reactor was 7 mm, and the mass of the catalyst was 0.2 g (20–40 mesh). The molar ratio of the feed CH_4/CO_2 was 1:1, and the space velocity (GHSV) of the gas mixture was fixed at 1.56×10^4 mL g^{-1} h^{-1}. Prior to reaction, catalysts were reduced at 650 °C for 4 h under hydrogen flow. The products were analyzed using on-line Agilent 6820 gas chromatography with a thermal conductivity detector and Ar gas was used as carrier gas.

The conversions of CH_4 and CO_2, the selectivities of H_2 and CO, and the ratio of H_2/CO were defined as follows:

$$X_{CH_4} = \frac{F_{CH_4,in} - F_{CH_4,out}}{F_{CH_4,in}}$$

$$X_{CO_2} = \frac{F_{CO_2,in} - F_{CO_2,out}}{F_{CO_2,in}}$$

$$S_{H_2} = \frac{F_{H_2,out}}{2(F_{CH_4,in} - F_{CH_4,out})}$$

$$S_{CO} = \frac{F_{CO,out}}{(F_{CH_4,in} - F_{CH_4,out}) + (F_{CO_2,in} - F_{CO_2,out})}$$

$$\frac{H_2}{CO} = \frac{S(H_2)}{S(CO)}$$

2.3. Catalyst characterization

Powder X-ray diffraction (XRD) experiments were conducted on a Bruker D8 Advance SS diffractometer equipped with a CuKα source (λ = 0.15432 nm) operated at 40 kV and 40 mA.

Nitrogen adsorption–desorption isotherms were measured on a Micromeritics ASAP 2010 apparatus. Before measurement, the samples were degassed at 110 °C for 3 h and then at 350 °C for 3 h under vacuum. The specific surface areas of the samples were calculated by the BET equation. The pore volumes were determined with the value of P/P_0 lower than 0.995.

The reducibility of catalysts was studied by hydrogen temperature-programmed reduction (TPR) on an AutoChem II 2920 apparatus equipped with a water trap. Prior to reduction, the sample (0.1 g) was pretreated in He with a flow velocity of 50 ml/min at room temperature. The TPR experiment was preformed under 10 vol.% H_2/Ar mixture with a flow velocity of 50 ml/min at a heating rate of 10 °C/min from room temperature to 800 °C. The consumption of hydrogen was monitored on-line with a build-in thermal conductivity detector (TCD).

X-ray photoelectron spectra (XPS) was recorded on a Thermo ESCALAB 250 spectrometer utilizing a Al Kα ($h\nu$ = 1486.6 eV) X-ray source. The spectra were acquired with an analyzer pass energy of 20 eV. All binding energies (BE) were referred to Si 2p line at 103.5 eV.

The amount of carbon deposition was analyzed by TGA2050 instrument. Catalyst samples were heated with the rate of 10 °C/min under air atmosphere from room temperature to 800 °C.

Fourier transform infrared spectra (FT-IR) were obtained with a Nicolet 380 spectrometer. The spectra were collected with 32 scans in a wave number range of 700–1500 cm^{-1} with a resolution of 4 cm^{-1}.

Transmission electron microscope (TEM) images were carried out on a Tecnai 20 S-TWIN instrument at 200 kV.

3. Results and discussion

3.1. Characterization of catalysts before reaction

Fig. 2 depicts the XRD patterns of Ni/KIT-6 and Ni-KIT-6 samples with different Ni contents. The small-angle XRD patterns of Ni-KIT-6 series samples are similar to that of KIT-6 [18], indicating the similar meso-structures. However, it is notable that there are progressive peak shift to low angle and magnitude decreases of characteristic peaks along with the increase of Ni content. This can be attributed to the participation of Ni species during the self-assembly of KIT-6 samples [19]. In addition, the XRD patterns of all samples exhibit a broad peak around 23°, which suggests an amorphous structure of the framework. Distinctly, there are three other peaks in the pattern of 6%Ni/KIT-6 which can be definitely ascribed to diffraction of NiO crystals. No obvious diffraction peaks

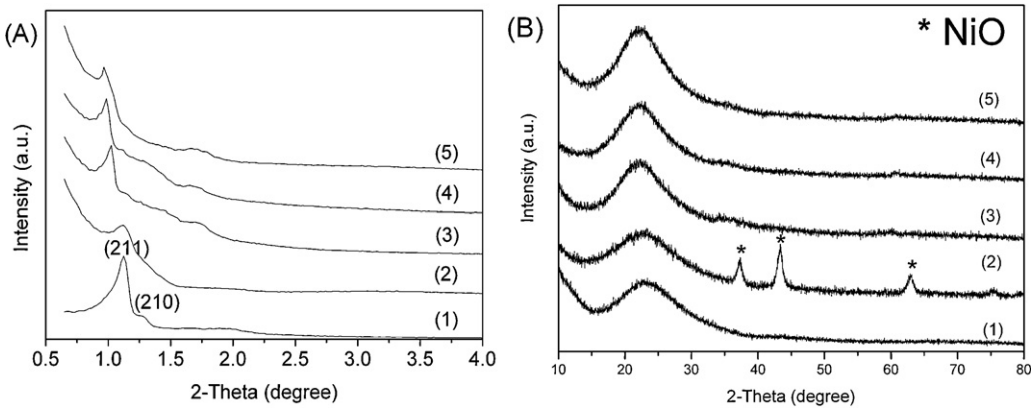

Fig. 2. (A) Small-angle and (B) wide-angle XRD patterns of (1) KIT-6, (2) 6%Ni/KIT-6, (3) 2%Ni-KIT-6, (4) 4%Ni-KIT-6, and (5) 6%Ni-KIT-6.

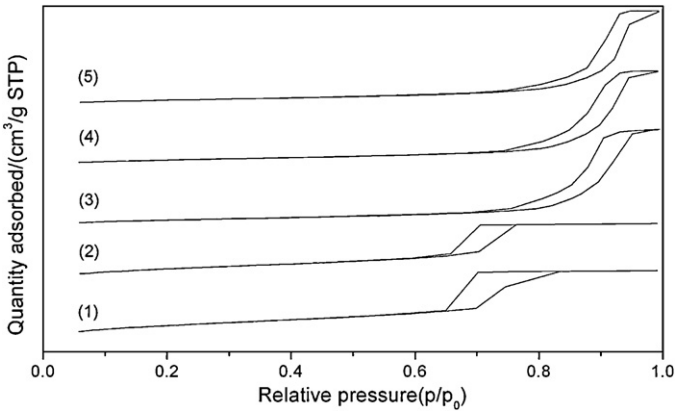

Fig. 3. N_2 adsorption/desorption isotherms of (1) KIT-6, (2) 6%Ni/KIT-6, (3) 2%Ni-KIT-6, (4) 4%Ni-KIT-6, and (5) 6%Ni-KIT-6.

of Ni oxide particles over the Ni-KIT-6 samples can be identified in all ranges of XRD patterns, indicating that there are small highly dispersed nano-crystals or even amorphous Ni oxide species over the Ni-KIT-6 samples.

The N_2 adsorption–desorption isotherms of Ni-KIT-6 and Ni/KIT-6 samples are shown in Fig. 3. All isotherms exhibit typical IV type isotherms with a H1 hysteresis loop in the relative pressure range of 0.6–1.0. Textural properties of the samples are listed in Table 1. After introducing nickel, an obvious decrease in surface area and an enlargement in pore diameter were observed. Such great differences between nickel-contained and non-nickel samples can be well explained by the isomorphous substitution of nickel atoms into silica frameworks, which leads to significant contraction of walls and consequently, expansion of pores [20].

The FT-IR spectra of Ni-KIT-6 and Ni/KIT-6 samples are shown in Fig. 4. The IR absorption peaks at 1089 cm^{-1} and 800 cm^{-1} are respectively assigned to asymmetric and symmetric vibrations of silica frameworks of KIT-6 [21]. Besides, compared with the spectra of 6%Ni/KIT-6 and KIT-6 samples, a red shift with value of ca. 10 cm^{-1} appears over the spectrum of Ni-KIT-6 at 1089 cm^{-1}, which is the definite perturbation of absorption peak. In addition, a lightly red shift and decrease for absorption peak at 965 cm^{-1}, which represent –Si–OH or Si–O–M vibration, can be observed for Ni-KIT-6 samples. This is believed to be the proofs of Ni atoms incorporation into the pore walls [22,23].

H_2-TPR profiles of two kinds of catalysts with the same Ni contents are shown in Fig. 5. For 6%Ni/KIT-6 sample, there are five reduction peaks centered at 314 °C, 398 °C, 534 °C, 606 °C and 750 °C respectively, and their peak area percentages are 27.9%, 40.8%, 14.5%, 5.2% and 11.6% respectively. According to references, the first peak, which possesses the greatest intensity, could be assigned to the reduction of bulky isolated Ni oxide particles, the next three peaks should be attributed to the reduction of Ni species on the pore wall surface and in the silica framework [15,24], and the last reduction peak at above 700 °C is mostly due to the reduction of small amount of Ni species stronger interacting with support, probably in the form of nickel silicates. In comparison, for the 6%Ni-KIT-6 sample, there are six reduction peaks centered at 260 °C, 422 °C, 510 °C, 574 °C, 660 °C and 758 °C respectively. Interestingly, the first reduction peak at 270 °C which is usually related to the reduction of smaller and better dispersed Ni oxide particles on the support surface [15,20,25], is much smaller than the one of 6%Ni/KIT-6 sample. Moreover, the next four broad reduction peaks between 350 °C and 700 °C which includes a new peak at 660 °C, could be assigned to the strong interaction of a large amount of Ni species with the support [15,25,26]. And they have higher integrated peak area percentage

Table 1
Textural properties and initial catalytic performances of different catalysts.

Sample	Surface area (m^2/g)[a]	Pore volume (mL/g)[b]	Pore diameter (nm)[b]	Carbon deposition (%)[c]
KIT-6	877.1	1.16	5.3	–
6%Ni/KIT-6	750.6	0.97	5.1	25.81
2%Ni-KIT-6	358.6	1.45	16.2	0.27
4%Ni-KIT-6	341.6	1.42	16.6	0.89
6%Ni-KIT-6	320.6	1.41	17.6	0.84

[a] Calculated by BET method.
[b] Calculated by BJH method.
[c] Carbon deposition of spent catalysts after 5 h of reaction at 800 °C calculated by difference of mass from 400 °C to 850 °C in TG.

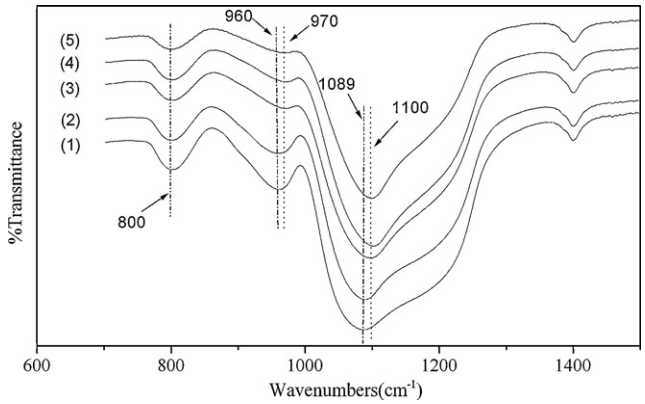

Fig. 4. FT-IR spectra of (1) KIT-6, (2) 6%Ni/KIT-6, (3) 6%Ni-KIT-6, (4) 4%Ni-KIT-6, and (5) 2%Ni-KIT-6.

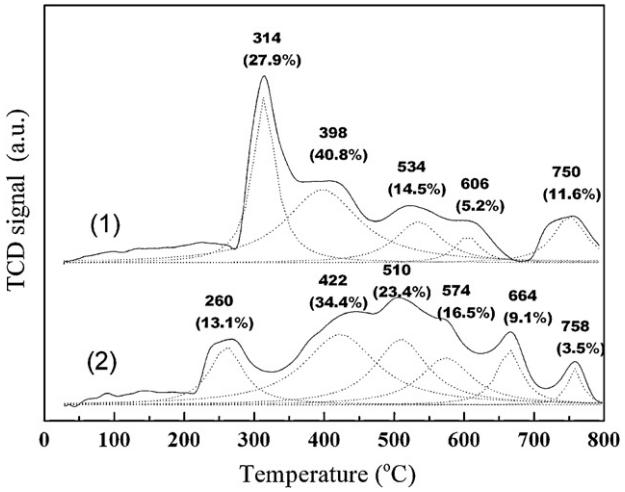

Fig. 5. H_2-TPR profiles of (1) 6%Ni/KIT-6 and (2) 6%Ni-KIT-6.

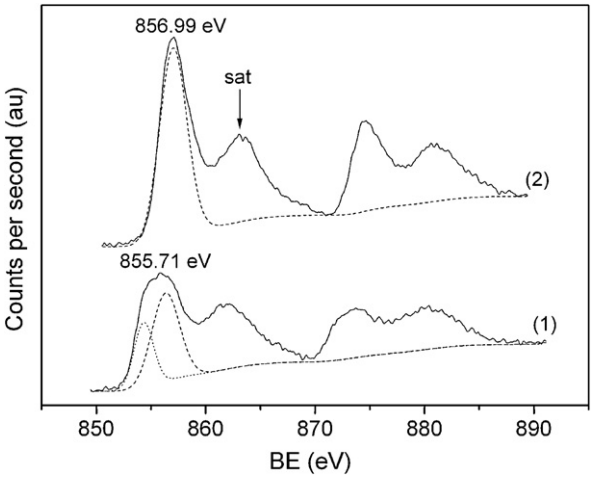

Fig. 6. XPS profiles of Ni 2p for (1) 6%Ni/KIT-6 and (2) 6%Ni-KIT-6.

than the 6%Ni/KIT-6 sample. These results indicate that the amount (corresponding to the peak area percentages) of Ni species with strong interaction to the support in the 6%Ni-KIT-6 is larger than the 6%Ni/KIT-6, which may have great effect on their Ni particle sizes after reduction and their catalytic performances.

The nature of surface Ni and Si elements of the 6%Ni-KIT-6 and 6%Ni/KIT-6 samples were detected by XPS in Fig. 6. The binding energy (BE) of Ni $2p_{3/2}$ for 6%Ni-KIT-6, which is located at 856.99 eV, could be assigned to the Ni^{3+} [22,27,28]. However, the BE of 6%Ni/KIT-6 shifted to the location at 855.71 eV, which indicates the simultaneous presence of Ni^{2+} [29] and Ni^{3+}. It is reported that the higher binding energy of Ni 2p of the samples produced by co-assembly method, the stronger interaction between the Ni species and the support, and consequently, the lower growth rate of nickel particles in high temperature [30]. Therefore, high anti-sinter properties are expected in the subsequent catalytic performance tests. In addition, all the spectra show primary satellite peaks close to 862.5 eV, which should be due to shake-up electrons [31].

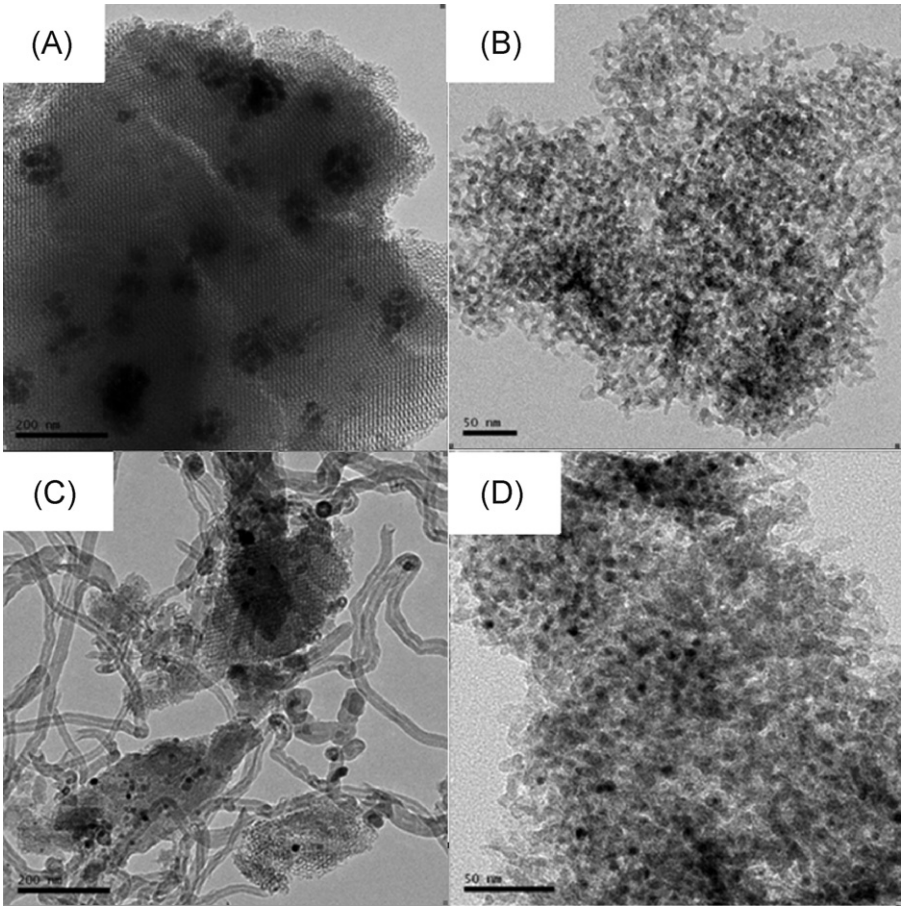

Fig. 7. TEM images of the fresh catalysts: (A) 6%Ni/KIT-6 reduced; (B) 6%Ni-KIT-6 reduced; and spent catalysts: (C) 6%Ni/KIT-6 and (D) 6%Ni-KIT-6 used as catalysts at 800 °C after 5 h, respectively. The scale bars in image (A–D) are 200, 50, 200 and 50 nm, respectively.

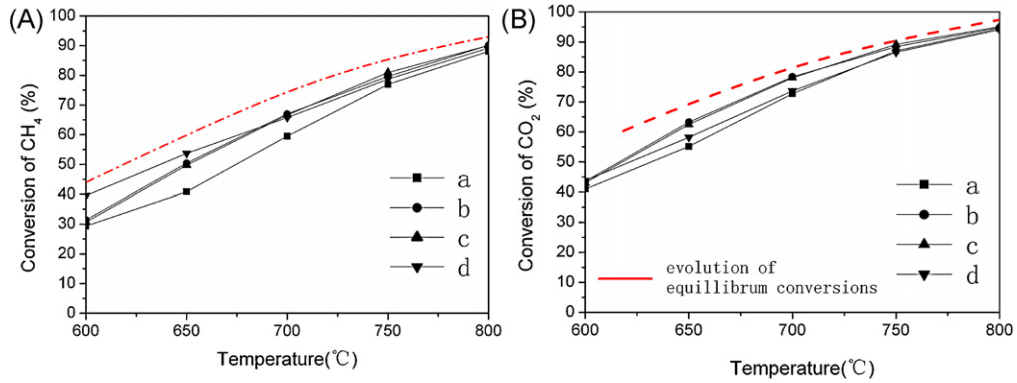

Fig. 8. Catalytic performance of different catalysts for CO_2 reforming of CH_4 at different reaction temperatures if considering the RWGS reaction: (a) 2%Ni-KIT-6, (b) 4%Ni-KIT-6, (c) 6%Ni-KIT-6, and (d) 6%Ni/KIT-6.

TEM observations were carried out on fresh reduced catalysts to identify the nickel particle size and distribution (Fig. 7A and C). It can be seen that there were nickel metal particles with the size of about 20–30 nm supported on the mesoporous silica matrix for 6%Ni/KIT-6 sample (Fig. 7A), and some agglomerates beyond mesopores can also be clearly observed. However, comparatively, nickel particles of 6%Ni-KIT-6 catalyst are estimated to be uniformly 3–5 nm (Fig. 7C), much smaller than the 6%/Ni/KIT-6 sample. Besides, these nickel particles are well dispersed without any agglomerates.

So, it can be concluded that different from Ni/KIT-6, there was stronger interaction between the Ni species and the support for Ni-KIT-6, and consequently it should have effect on its reduction of Ni species to nickel metal, which may result in its smaller and more uniform nickel metal particles.

3.2. Catalytic performance

Fig. 8 shows the initial catalytic performances of various catalysts at different temperatures. All catalysts exhibit relatively low catalytic activities at 600 °C and a progressive increase of both CH_4 and CO_2 conversions with the reaction temperature rising. Meanwhile, 2%Ni-KIT-6 shows lower conversion than the others at all temperatures, indicating that increasing Ni content can improve the catalytic activity. The evolution curve of thermodynamic equilibrium conversions of CH_4/CO_2 in different temperatures have also been calculated and graphed in Fig. 8. It is found that conversions of CH_4/CO_2 are a little lower than their equilibrium conversions at all tested temperatures if considering the RWGS reaction. Under these reaction conditions, 4% and 6%Ni-KIT-6 possess almost the same catalytic evolution curves which means

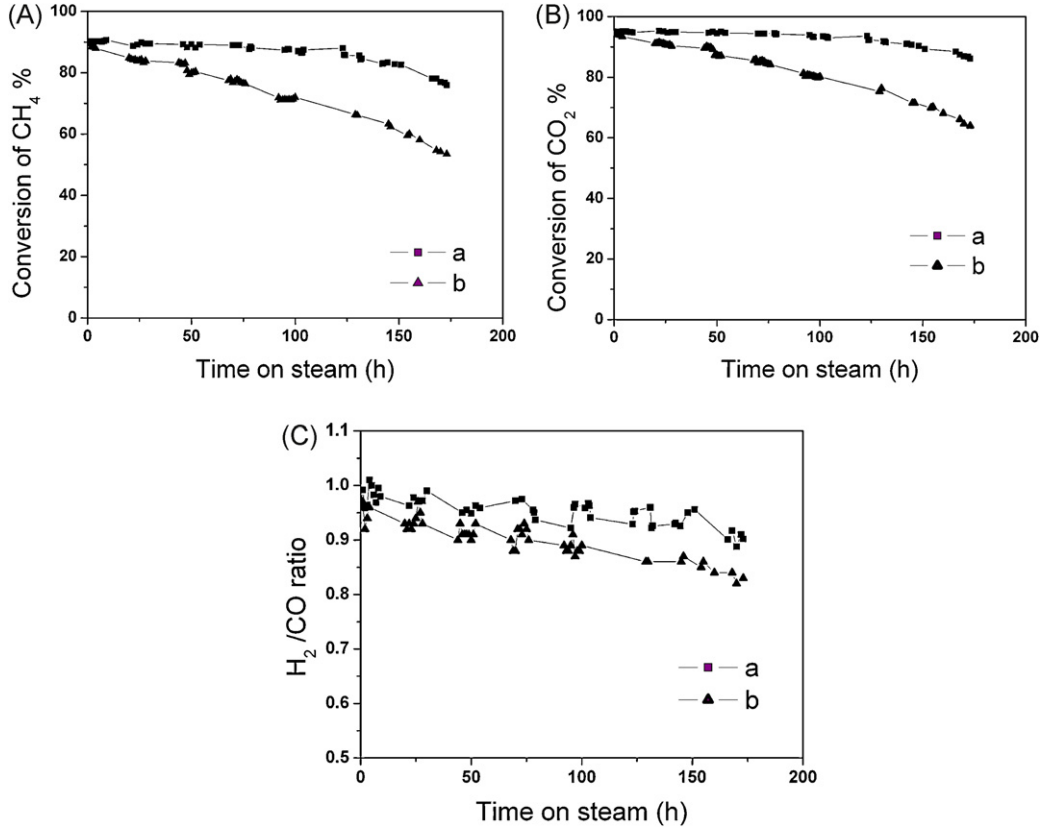

Fig. 9. The evolution of CH_4 (A) conversions, CO_2 (B) conversions and H_2/CO ratios (C) over various catalysts at 800 °C: (a) 6%Ni-KIT-6 and (b) 6%Ni/KIT-6.

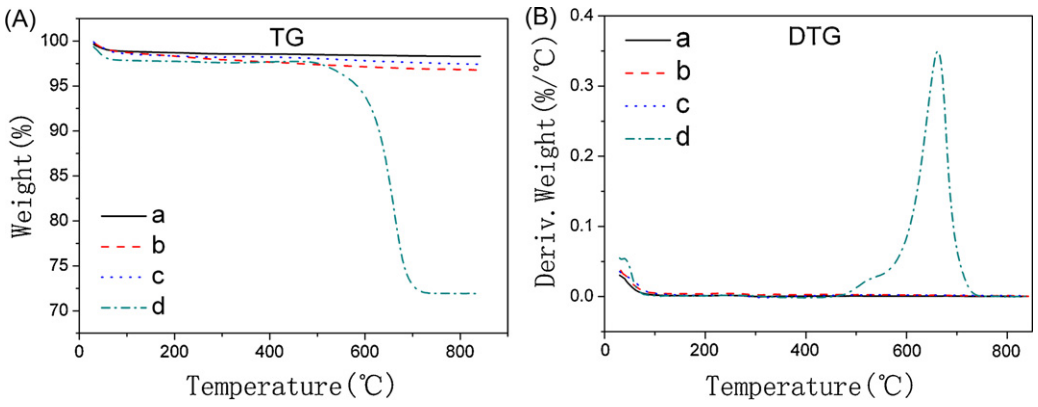

Fig. 10. TG and DTG profiles of different catalysts after 5 h reaction: (a) 2%Ni-KIT-6, (b) 4%Ni-KIT-6, (c) 6%Ni-KIT-6, and (d) 6%Ni/KIT-6.

overloaded Ni contents are useless to the improvement of catalytic properties.

To compare the catalytic stabilities and lifetimes of 6%Ni-KIT-6 and 6%Ni/KIT-6 catalysts, activity testings as long as about 180 h were performed and the results are shown in Fig. 9. It is apparent that although both catalysts have almost the same initial activity, 6%Ni-KIT-6 suffered from a much slower deactivation rate than the 6%Ni/KIT-6 sample. It can be seen that before 100 h there was almost no significant activity loss for 6%Ni-KIT-6, and after 100 h its deactivation became more and more apparent. While for 6%Ni/KIT-6, a much faster deactivation rate can be identified.

In addition, the H_2/CO ratios for both catalysts are between 0.8 and 1, a little smaller than the stoichiometric ratio of dry reforming reaction. This small differences should be related to the reverse water–gas shift reaction (RWGS) [20,31,32], the side reaction of the reactant CO_2 with the product H_2. Moreover, it can be seen that H_2/CO ratio for 6%Ni-KIT-6 was also higher than 6%Ni/KIT-6. From the thermodynamic equilibrium calculation of dry reforming together with RWGS reaction, it is known that more conversions of CH_4/CO_2 always produce greater H_2/CO mole ratios which also consequently exhibited the performance difference between the impregnated and co-assembled catalysts.

The excellent anti-deactivation properties and high catalytic efficiency of 6%Ni-KIT-6 sample may be closely related to its extremely small and uniform nickel metal particles mentioned above.

3.3. *Deactivation analysis of catalysts*

The carbon deposition of spent catalysts after reaction for 5 h was calculated by TG/DTG profiles, which were shown in Fig. 10 and listed in Table 1 in detail. Generally, the appearance of low-temperature loss around 100 °C is associated with the desorption of moisture, e.g. H_2O. The weight losses from 100 °C to 400 °C are usually caused by the oxidation of active carbon or amorphous carbon [14], and the graphitic carbon oxidizes after 400 °C. From the TG/DTG profiles, it is clear that a massive amount of graphitic carbon deposition appeared on the impregnated samples, but only insignificant carbon deposition exists for Ni-KIT-6 series samples. Such different quantities of coke formation, according to previous reports [33–35], suggests quick deactivation of Ni/KIT-6, and comparatively, outstanding anti-deactivation properties of Ni-KIT-6 series samples.

To further identify the carbon deposition of spent catalysts by impregnated and incorporation methods respectively, TEM tests were carried out and the images are shown in Fig. 7C and D. For the impregnated catalyst, 6%Ni/KIT-6, after being used in dry reforming for 5 h, the carbon nanotube/fiber can be easily found in the TEM image (Fig. 7C), but no significant carbon particles can be recognized for Ni-KIT-6 (Fig. 7D). Such results can be confirmed by XRD patterns (not shown), in which only 6%Ni/KIT-6 shows obvious diffraction peaks of graphitic carbon. Therefore, the incorporation method surpass the conventional route in prompting the Ni species to be smaller size and higher dispersive, preventing the catalyst from sintering in the mesopore networks, and consequently, leading to less carbon deposition and a prolonged lifetime in the dry reforming reactions.

4. Conclusions

In conclusion, a kind of Ni-doped mesoporous material, Ni-KIT-6, was synthesized by one-spot co-assembly method during which Ni species were homogeneously incorporated into the pore walls. After calcination, the nickel oxide, with particle size less than 5 nm, presents wonderful dispersive distribution in the pore walls. In the dry reforming reaction, the catalyst can effectively restrain active metal sintering and carbon deposition due to its unique mesoporous structure and good dispersive distribution of Ni species, which consequently lead to higher activity and prolonged lifetime when compared with the catalyst prepared by conventional incipient wetness impregnation method.

Acknowledgment

Financial support from Major State Basic Research Development Program of China (grants 2009CB623506), National Natural Science Foundation of China (Application code: B060904) and Shanghai Postdoctoral Scientific Program (No. 12R21422000) are greatly acknowledged.

References

[1] C.S. Song, Catalysis Today 115 (2006) 2–32.
[2] G. Bonura, C. Cannilla, F. Frusteri, Applied Catalysis B 121–122 (2012) 135–147.
[3] M.C.J. Bradford, M.A. Vannice, Catalysis Reviews: Science and Engineering 41 (1999) 1–42.
[4] M.S. Fan, A.Z. Abdullah, S. Bhatia, ChemCatChem 1 (2009) 192–208.
[5] S. Tang, L. Ji, J. Lin, H.C. Zeng, K.L. Tan, K. Li, Journal of Catalysis 194 (2000) 424–430.
[6] X.L. Zhu, P.P. Huo, Y.P. Zhang, D.G. Cheng, C.J. Liu, Applied Catalysis B 81 (2008) 132–140.
[7] S.Y. Shang, G.H. Liu, X.Y. Chai, X.M. Tao, X. Li, M.G. Bai, W. Chu, X.Y. Dai, Y.X. Zhao, Y.X. Yin, Catalysis Today 148 (2009) 268–274.
[8] M. Rezaei, S.M. Alavi, S. Sahebdelfar, P. Bai, X.M. Liu, Z.F. Yan, Applied Catalysis B 77 (2008) 346–354.
[9] W. Hua, L. Jin, X. He, J. Liu, H. Hu, Catalysis Communications 11 (2010) 968–972.
[10] M.-S. Fan, A.Z. Abdullah, S. Bhatia, Applied Catalysis B 100 (2010) 365–377.
[11] Y.X. Pan, C.J. Liu, P. Shi, Journal of Power Sources 176 (2008) 46–53.

[12] M. Rezaei, S.M. Alavi, S. Sahebdelfar, Z.F. Yan, Energy & Fuels 22 (2008) 2195–2202.
[13] S. Wang, Studies in Surface Science and Catalysis 165 (2007) 795–798.
[14] D. Liu, X.Y. Quek, H.H.A. Wah, G. Zeng, Y. Li, Y. Yang, Catalysis Today 148 (2009) 243–250.
[15] X.Y. Quek, D. Liu, W.N.E. Cheo, H. Wang, Y. Chen, Y. Yang, Applied Catalysis B 95 (2010) 374–382.
[16] S. Zhang, J. Wang, H. Liu, X. Wang, Catalysis Communications 9 (2008) 995–1000.
[17] H.S. Bengaard, J.K. Nørskov, J. Sehested, B.S. Clausen, L.P. Nielsen, A.M. Molenbroek, J.R. Rostrup-Nielsen, Journal of Catalysis 209 (2002) 365–384.
[18] F. Kleitz, S.H. Choi, R. Ryoo, Chemical Communications 17 (2003) 2136–2137.
[19] K. Soni, B.S. Rana, A.K. Sinha, A. Bhaumik, M. Nandi, M. Kumar, G.M. Dhar, Applied Catalysis B 90 (2009) 55–63.
[20] D. Liu, R. Lau, A. Borgna, Y. Yang, Applied Catalysis A 358 (2009) 110–118.
[21] E.C. Chetty, S. Maddila, C. Southway, S.B. Jonnalagadda, Industrial & Engineering Chemistry Research 51 (2012) 2864–2873.
[22] Y.H. Ikuhara, T. Saito, S. Takahashi, Y. Sasaki, T. Hirayama, Journal of the American Ceramic Society 95 (2012) 524–529.
[23] Y.F. Shao, L.Z. Wang, J.L. Zhang, M. Anpo, Journal of Physical Chemistry B 109 (2005) 20835–20841.
[24] B.S. Liu, C.T. Au, Applied Catalysis A 244 (2003) 181–195.
[25] H. Wan, X. Li, S. Ji, B. Huang, K. Wang, C. Li, Journal of Natural Gas Chemistry 16 (2007) 139–147.
[26] Y. Yang, S. Lim, G. Du, Y. Chen, D. Ciuparu, G.L. Haller, Journal of Physical Chemistry B 109 (2005) 13237–13246.
[27] T.L. Barr, Journal of Physical Chemistry 82 (1978) 1801–1810.
[28] D. Briggs, M.P. Seah, Practical Surface Analysis, vol. 1, 2nd ed., John Willey & Sons, 1993.
[29] J.-G. Kim, D.L. Pugmire, D. Battaglia, M.A. Langell, Applied Surface Science 165 (2000) 70–84.
[30] Z.M. Cui, S.P. Jiang, C.M. Li, Chemical Communications 47 (2011) 8418–8420.
[31] A. Goguet, F. Meunier, J.P. Breen, R. Burch, M.I. Petch, A.F. Gheciu, Journal of Catalysis 226 (2004) 382–392.
[32] B.A. Peppley, J.C. Amphlett, L.M. Keams, R.F. Mann, Applied Catalysis A 179 (1999) 21–29.
[33] Z.L. Zhang, X.E. Verykios, Catalysis Today 21 (1994) 589–595.
[34] B.S. Liu, C.T. Au, Catalysis Letters 85 (2003) 165–170.
[35] W.D. Zhang, B.S. Liu, C. Zhu, Y.L. Tian, Applied Catalysis A 292 (2005) 138–143.